Earthq Eng & Eng Vib (2014) 13: 101-111 **DOI**: 10.1007/s11803-014-0215-3

Structural modal parameter identification and damage diagnosis based on Hilbert-Huang transform

Han Jianping†, Zheng Peijuan‡ and Wang Hongtao‡

Key Laboratory of Disaster Prevention and Mitigation in Civil Engineering of Gansu Province, Lanzhou University of Technology, Lanzhou 730050, China

Abstract: Traditional modal parameter identification methods have many disadvantages, especially when used for processing nonlinear and non-stationary signals. In addition, they are usually not able to accurately identify the damping ratio and damage. In this study, methods based on the Hilbert-Huang transform (HHT) are investigated for structural modal parameter identification and damage diagnosis. First, mirror extension and prediction via a radial basis function (RBF) neural network are used to restrain the troublesome end-effect issue in empirical mode decomposition (EMD), which is a crucial part of HHT. Then, the approaches based on HHT combined with other techniques, such as the random decrement technique (RDT), natural excitation technique (NExT) and stochastic subspace identification (SSI), are proposed to identify modal parameters of structures. Furthermore, a damage diagnosis method based on the HHT is also proposed. Time-varying instantaneous frequency and instantaneous energy are used to identify the damage evolution of the structure. The relative amplitude of the Hilbert marginal spectrum is used to identify the damage location of the structure. Finally, acceleration records at gauge points from shaking table testing of a 12-story reinforced concrete frame model are taken to validate the proposed approaches. The results show that the proposed approaches based on HHT for modal parameter identification and damage diagnosis are reliable and practical.

Keywords: modal parameter identification; damage diagnosis; Hilbert-Huang transform; natural excitation technique; stochastic subspace identification; random decrement method; shaking table test

1 Introduction

Identifying modal parameters and damage via processing vibration signals is one of the mainstream approaches for structural health monitoring and damage diagnosis. The methods of damage diagnosis by monitoring the changes in the dynamic properties (frequencies, mode shapes and modal damping) of structures have received considerable attention (Doebling *et al*., 1996; Curadelli *et al*., 2008).

The traditional processing approaches based on Fourier analysis are not capable of dealing with nonlinear and non-stationary signals. Furthermore, most of traditional identification methods suffer from low precision in identifying damping ratios. They also have practical limitations in variation of modal parameters, which are insensitive to damage development. For example, from tests on a bridge, Farrar and Jauegui (1998) concluded that for a reduction in the bending stiffness of the overall bridge with 21% cross section, no significant reduction in the modal frequencies was observed. Chen *et al*. (2005), based on the observation of changes in natural frequencies of steel space structures subjected to atmospheric corrosion, found that atmospheric corrosion does not perceptibly affect the natural frequencies of the structure.

The advanced time-frequency analysis methods, such as wavelet transform (WT) and Hilbert-Huang transform (HHT), have been rapidly developing in recent years in structural health monitoring (SHM) of civil engineering structures. These methods are suitable for processing nonlinear and non-stationary signals. HHT is capable of decomposing a signal more precisely than wavelet analysis because the former provides multi-resolution in various frequency scales and takes the signal frequency contents and their variation into consideration. In addition, the HHT has an adaptive nature in analyzing the nonlinear and non-stationary data that is not available in Wavelet transform. Due to these features, the HHT is much more attractive and has already been applied in many fields, such as ocean, earthquake, biology and structural health monitoring (Huang *et al*., 1998). It consists of two main parts, namely empirical mode decomposition (EMD) and

Correspondence to: Han Jianping, Key Laboratory of Disaster Prevention and Mitigation in Civil Engineering of Gansu Province, Lanzhou University of Technology, Lanzhou 730050, China
Tel: +86 -931-2976066; Fax: +86-931-2976066
E-mail: jphan@lut.cn
†Professor; ‡Master

Supported by: Gansu Science and Technology Key Project under Grant No. 2GS057-A52-008
Received May 18, 2012; **Accepted** November 11, 2013

Hilbert transform (HT). And the crucial step is EMD, by which any vibration signal can be decomposed into several intrinsic mode functions (IMFs). Each IMF is a mono-component and can be treated as an approximate modal response. The analytical signal is constructed via HT and then the instantaneous characteristics of the signal are obtained. However, there is a troublesome end-effect issue in the EMD process resulting in an error in each decomposed component. In this study, mirror extension and prediction via radial basis function (RBF) neural networks are proposed to restrain the end-effect issue.

A modal parameter identification method using the HHT is based on the free-decay response or impulse response of an SDOF system. Generally, the measured data are the responses obtained under random excitation. Each IMF obtained from the EMD is a modal response component of the structure, which is not an ideal free-decay response. It consists of free-decay response and forced vibration response induced by external excitation (Yang and Lei, 2000). The accuracy of the approach based on EMD, random decrement technique (RDT) and Ibrahim Time Domain (ITD) in identifying natural frequencies and damping ratios has been verified to be remarkable (Liu *et al*., 2012). In this study, for each obtained IMF, RDT is applied to obtain the free-decay response of the corresponding mode. Alternatively, the natural excitation technique (NExT) is applied to obtain the impulse response of the corresponding mode. Then, for the obtained free-decay response or impulse response, the analytical signal is built via the HT to identify the modal parameters.

In addition, although the stochastic subspace identification (SSI) method is viewed as an advanced modal parameter identification method in the time domain, it also has some drawbacks. For example, the stabilization diagram from SSI is not clear and the stable pole is scattered due to the interference of other modal components and unwanted noise (Yu and Ren, 2005). In order to overcome this problem, an approach based on the EMD is proposed to improve the results identified from the SSI method.

Finally, the approaches based on HHT to identify the damage evolution and damage location are also proposed. When the structure is subjected to damage, the instantaneous frequency of the structure and the interior energy distribution of the structure will both change. The sensitivity of HHT for initial damage detection was examined by Hsu *et al*. (2013) and the results show that the HHT is a powerful method for analyzing the acceleration data for steel structures with initial damage from earthquakes. In this study, the time-varying instantaneous frequency and Hilbert instantaneous energy obtained by the HT are used to identify the damage evolution, and the relative amplitude of Hilbert marginal spectrum is used to identify the damage location. Finally, all the proposed approaches are validated via case studies of acceleration records from the shaking table tests of a 12-story reinforced concrete frame model.

2 Brief description of the Hilbert-Huang transform (HHT)

2.1 Empirical mode decomposition

The EMD is the crucial step of the HHT. It is based on the assumption that any complex time-series is composed of intrinsic mode functions which are different, simple and non-sinusoidal. Using EMD, any of the original time-series $x(t)$ can be decomposed into n IMFs and a residual (Huang *et al*., 1998; Rilling *et al*., 2003).

$$x(t) = \sum_{j=1}^{n} C_j(t) + r_n(t) \tag{1}$$

where $C_j(t)$ for j=1,…, n are IMFs of the original signal $x(t)$, and $r_n(t)$ is the residual.

Each IMF represents the time-series with a different characteristic scale. Thus, the whole process is the superposition of fluctuations with different characteristic scales.

However, in the EMD, the $C_j(t)$ component has unavoidable error because of the influence of the end-effect issue. In the process of the EMD, it is necessary to fit all maxima and minima with cubic splines to construct the upper and lower envelopes of the signal. However, there are some practical difficulties in dealing with the boundaries of the signal. Furthermore, because the subsequent IMF components are decomposed based on the previous IMF components and the residual, the error that existed in the previous decomposition will propagate into the later decomposition. Thus with the decomposition process, the error generated from the end swings can eventually propagate inwards and corrupt the whole signal, especially in the low frequency components. As a result, the IMFs will be unreliable in the serious cases.

In this study, mirror extension and prediction via a radial basis function (RBF) neural network are proposed to restrain the end-effect issue in EMD (Han *et al*., 2010):

(1) Mirror extension. First, partial curves near to the right and left ends and corresponding extrema are investigated and the locations for the mirrors are decided according to distribution characteristics of the curve. For example, one mirror is placed on the l-th and another on the r-th extreme point located at the left and right end of the signal, respectively. Then, the signal between the two mirrors is mapped outwards and the periodical signal, which is twice as long as the signal between the two mirrors, will be obtained. The signal after the mirror extension is periodical and does not contain the end points of the original signal.

(2) RBF neural network prediction. The prediction proceeded by the characteristics of the whole time series and specific form of time series on the endpoints to

obtain extreme values. The first step is a learning process and the second is an extending process. The basic idea of an RBF neural network is to use the radial basis function as the base of the hidden layer to constitute the hidden layer space. Thus, the input vector is directly mapped to the hidden layer space and this mapping relationship will be confirmed while the center of the radial basis function is determined. The mapping from the hidden layer space to the input layer space is linear and the network output is the linear weighted summation of the hidden layer outputs.

2.2 Hilbert transform (HT)

For a given signal $x(t)$, its HT can be expressed as

$$y(t) = HT[x(t)] = \frac{1}{\pi} P\int_{-\infty}^{+\infty} \frac{x(\tau)}{t-\tau}\mathrm{d}\tau \tag{2}$$

where P indicates the Cauchy principal value.

Thus, the analytical signal can be constructed as

$$Z(t) = x(t) + \mathrm{i}y(t) = A(t)\mathrm{e}^{\mathrm{i}\theta(t)} \tag{3}$$

in which

$$A(t) = A_0\mathrm{e}^{\mathrm{i}\omega t},\ \theta(t) = \omega t - \alpha \tag{4}$$

$$\omega(t) = \mathrm{d}\theta(t)/\mathrm{d}t \tag{5}$$

From the equations above, the instantaneous amplitude, the instantaneous phase and the instantaneous frequency can be obtained.

The amplitude of the frequency-time decomposition of $x(t)$, that is the Hilbert-Huang spectrum of $x(t)$, is given by

$$A(t,\omega;x) = \sum_{j=1}^{n} A_j(t,\omega_j) \tag{6}$$

where $A_j(t, \omega_j)$ is the instantaneous amplitude of the jth IMF at time t with frequency ω_j.

Hilbert marginal spectrum $h(\omega, x)$ can be obtained by integrating the amplitude $A(t, \omega; x)$ with respect to time,

$$h(\omega,x) = \int_0^T A(t,\omega;x)\mathrm{d}t \tag{7}$$

Hilbert instantaneous energy $IE(t)$ can be obtained by integrating the square of amplitude with respect to frequency,

$$IE(t) = \int_\omega A^2(t,\omega;x)\mathrm{d}\omega \tag{8}$$

3 Brief introduction of RDT, NExT and SSI

3.1 Random decrement technique (RDT)

RDT is a time domain signal processing approach which is developed to construct a characteristic signal from the ensemble average of sample segments preselected from random response signals (Ibrahim, 1977).

For a single degree of freedom (SDOF) linear system, forced vibration response of a test point under random excitation can be expressed as

$$y(t) = y(0)D(t) + \dot{y}(0)V(t) + \int_0^t h(t-\tau)f(\tau)\mathrm{d}\tau \tag{9}$$

in which $D(t)$ is the free vibration response of system with initial displacement 1 and initial velocity 0, $V(t)$ is the free vibration response of system with initial displacement 0 and initial velocity 1, $y(0)$ and $\dot{y}(0)$ are the initial displacement and initial velocity of the system, respectively, $h(t)$ is the unit impulse response function of the system, and $f(t)$ is the external excitation.

An appropriate parameter is adopted to eliminate the vibration response $y(t)$ of the system. The response displacement $y(t\text{-}t_i)$ starting from time t_i can be expressed as follows:

$$y(t-t_i) = y(t_i)D(t-t_i) + \dot{y}(t_i)V(t-t_i) + \int_{t_i}^t h(t-\tau)f(\tau)\mathrm{d}\tau \tag{10}$$

After moving the initial time point at t_1 to the origin coordinate, a series of function $x_i(t)$=(i=1,2,...N) can be given as follows:

$$x_i(t) = AD(\mathrm{t}) + \dot{y}(t_i)V(t) + \int_0^t h(t-\tau)f(\tau)\mathrm{d}\tau \tag{11}$$

Then, the statistical average of $x_i(t)$ is calculated and the following equation is obtained,

$$\begin{aligned} x(t) &= \frac{1}{N}\sum_{i=1}^{N} x_i(t) \\ &\approx \mathrm{E}\left[AD(t) + \dot{y}(t_i)V(t) + \int_0^t h(t-\tau)\mathrm{d}\tau\right] \\ &\approx AD(t) + \mathrm{E}[\dot{y}(t_i)]V(t) + \int_0^t h(t-\tau)\mathrm{E}[f(\tau)]\mathrm{d}\tau \end{aligned} \tag{12}$$

in which $f(t)$ is the stationary random excitation with zero mean value, and $y(t)$ is the vibration response of the system. $\dot{y}(t_i)$ is also the stationary random process with zero mean value.

Finally, the free vibration response can be obtained as

$$x(t) = AD(t) \tag{13}$$

in which A is the initial displacement of $x(t)$.

3.2 Natural excitation technique (NExT)

In the NExT process, the impulse response function is replaced by the cross-correlation function of the responses of the linear system at two points under white noise excitation (Caicedo *et al*., 2004).

For a linear system with N degrees of freedom, when the kth point of system is subjected to the excitation $f_k(t)$, the response at the ith point $x_{ik}(t)$ can be expressed as

$$x_{ik}(t) = \sum_{r=1}^{2N} \phi_{ir}a_{kr}\int_{-\infty}^{t} \mathrm{e}^{\lambda r(t-p)}f_k(p)\mathrm{d}p \tag{14}$$

where ϕ_{ir} is the rth mode displacement at the ith point and a_{kr} is the constant only related to k and r.

When the kth point of the system is subjected to the unit impulse excitation, the impulse response function $h_{ik}(t)$ at the ith point can be expressed as

$$h_{ik}(t)=\sum_{r=1}^{2N}\phi_{ir}a_{kr}\mathrm{e}^{\lambda_r t} \tag{15}$$

Cross-correlation function of the response $x_{ik}(t)$ and $x_{jk}(t)$at the ith and jth points under the excitation $f_k(t)$ can be expressed as

$$R_{ijk}(\tau)=\mathrm{E}\left[x_{ik}(t+\tau)x_{jk}(t)\right]=\sum_{r=1}^{2N}\sum_{s=1}^{2N}\phi_{ir}\phi_{js}a_{kr}a_{ks}\cdot$$
$$\int_{-\infty}^{t}\int_{-\infty}^{t+\tau}\mathrm{e}^{\lambda_r(t+\tau-p)}\mathrm{e}^{\lambda_s(t-q)}\mathrm{E}\left[f_k(p)f_k(q)\right]\mathrm{d}p\mathrm{d}q \tag{16}$$

If the excitation $f_k(t)$ is the ideal white noise, the equation $\mathrm{E}\left[f_k(p)f_k(q)\right]=a_k\delta(p-q)$ can be obtained, in which δ is the unit impulse excitation and a_k is the constant related to k only. Thus, $R_{ijk}(\tau)$ can be expressed as follows:

$$R_{ijk}(\tau)=\sum_{r=0}^{2N}b_{jr}\phi_{ir}\mathrm{e}^{\lambda_r r},$$
$$b_{jr}=\sum_{s=1}^{2N}\phi_{js}\mathrm{e}^{\lambda_r r}a_{kr}a_{ks}a_k\left(-\frac{\mathrm{e}^{\lambda_r r}}{\lambda_r+\lambda_s}\right)jr \tag{17}$$

3.3 Stochastic subspace identification (SSI)

SSI is a relatively advanced time domain method for modal parameter identification under ambient excitation. Its mathematical model is constructed by the state space equation. The modal parameters of the system are obtained by solving the system matrix and output matrix of the state space equation (Van and De Moor, 1996).

In the process of sampling signals, after sampling discretely and introducing random noise, a continuous state-space equation turns into a discrete random state-space equation,

$$\begin{cases}\boldsymbol{x}_{k+1}=\boldsymbol{A}\boldsymbol{x}_k+\boldsymbol{B}\boldsymbol{u}_k+\boldsymbol{w}_k\\ \boldsymbol{y}_k=\boldsymbol{C}\boldsymbol{x}_k+\boldsymbol{D}\boldsymbol{u}_k+\boldsymbol{v}_k\end{cases} \tag{18}$$

in which $\boldsymbol{x}_k=\boldsymbol{x}(k\Delta t)$ is the discrete state vector, and $\boldsymbol{y}_k=\boldsymbol{y}(k\Delta t)$ and $\boldsymbol{u}_k=\boldsymbol{u}(k\Delta t)$ are the discrete input vector and the discrete output vector, respectively. $\boldsymbol{A}=e^{\boldsymbol{A}_c\Delta t}$ is the discrete state matrix, and $\boldsymbol{B}=[\boldsymbol{A}-\boldsymbol{I}]\boldsymbol{A}_c^{-1}\boldsymbol{B}_c$ is the input influence matrix, $\boldsymbol{C}$ is the output influence matrix, $\boldsymbol{D}$ is the direct transmission matrix, $\boldsymbol{w}_k$ is the process noise and $\boldsymbol{v}_k$ is the measurement noise. $\boldsymbol{w}_k$ and $\boldsymbol{v}_k$ are assumed to be two correlated zero-mean Gaussian white noise processes, defined by their covariance matrices as

$$\mathrm{E}\left[\begin{pmatrix}\boldsymbol{w}_p\\ \boldsymbol{v}_p\end{pmatrix}\begin{pmatrix}\boldsymbol{w}_q^{\mathrm{T}} & \boldsymbol{v}_q^{\mathrm{T}}\end{pmatrix}\right]=\begin{pmatrix}\boldsymbol{Q} & \boldsymbol{S}\\ \boldsymbol{S}^{\mathrm{T}} & \boldsymbol{R}\end{pmatrix}\delta_{pq} \tag{19}$$

in which E is the mathematic expectation and δ_{pq} is the Kronecker delta function.

For Eq. (18), if the input term $\boldsymbol{u}_{\mathrm{k}}$ can be merged with the noise terms $\boldsymbol{w}_k$ and $\boldsymbol{v}_k$, the discrete-time stochastic state-space model of a vibrating structure is obtained,

$$\begin{cases}\boldsymbol{x}_{k+1}=\boldsymbol{A}\boldsymbol{x}_k+\boldsymbol{w}_k\\ \boldsymbol{y}_k=\boldsymbol{C}\boldsymbol{x}_k+\boldsymbol{v}_k\end{cases} \tag{20}$$

4 Modal parameter identification approaches based on HHT

4.1 Modal frequency identification using HHT

From the Fourier spectrum of the acceleration response $x(t)$, the range of each modal frequency can be determined approximately, i.e., $\omega_{j\mathrm{L}}<\omega_j<\omega_{j\mathrm{H}}$. First, $x(t)$ is processed through the band-pass filters with a frequency band $\omega_{j\mathrm{L}}<\omega_j<\omega_{j\mathrm{H}}$. Then, the signal obtained from the jth band-pass filter is processed through EMD, and the resulting first IMF is quite close to the jth modal response. Repeating the same procedures for j = 1,2,...,n, n modal responses can be obtained.

By performing HT for each modal response, the analytical signal is constructed. Based on Eq. (3), the plot of the phase angle $\theta_j(t)$ vs. time t is fitted by a straight line using the linear least-square fit procedure. Then, the slope of the fitted straight line is the modal frequency ω_j.

4.2 Modal parameter identification using HHT and NExT or RDT

The method using HHT and NExT or RDT is that each modal response is obtained through a band-pass filter and EMD is used to first obtain the free-decay response via RDT or NExT. Then, the free-decay response is adopted to perform HT in order to identify modal parameters. The procedure for identifying modal parameters using HHT and NExT or RDT is explained as follows.

First, for each modal response $x'_j(t)$ obtained from EMD, the free-decay response $x''_j(t)$ is obtained by using RDT or NExT. Then, it can be expressed as follows:

$$x''_j(t)=R_j\mathrm{e}^{-\zeta_j\omega_j t}\cos(\omega_{\mathrm{d}j}t-\theta_j) \tag{21}$$

HT is conducted for the equation above and then analytical signal $Y_j(t)$ is constructed,

$$Y_j(t)=A_j(t)\mathrm{e}^{\mathrm{i}\theta_j(t)}=R_j\mathrm{e}^{-\zeta_j\omega_j t}\mathrm{e}^{\mathrm{i}(\omega_{\mathrm{d}j}t-\theta_j)} \tag{22}$$

The natural logarithm of the decaying amplitude $A_j(t)$ in the above equation can be written as follows:

$$\ln A_j(t)=-\zeta_j\omega_j t+\ln R_j \tag{23}$$

Then, the plot of $A_j(t)$ vs. time t is fitted by a straight line using the linear least-square fit procedure. $\zeta_j\omega_j$ can be estimated from the slope of the fitted straight line. Damping ratio ξ_j of the jth mode can be obtained because the modal frequency ω_j is already known.

4.3 Modal parameter identification using EMD and SSI

The rationale of the modal parameter identification approach using EMD and SSI is different from the rationale of the identification approach using HHT and NExT or RDT. As mentioned before, SSI is an advanced time-domain approach to analyze the response signal. It is based on a time-invariant linear state space model and the modal parameters are identified by solving the state matrix and output matrix of the state space equation via some effective mathematical tools, such as QR decomposition of the matrix, singular value decomposition and least squares. However, it is difficult to identify modal parameters accurately using only SSI because the input is assumed to be white noise and the stability diagram of SSI includes modal information of all orders.

The approach using EMD and SSI is that the original response data are dealt with EMD first to obtain the single modal response. Then, the signal obtained through EMD is used to identify modal parameters using SSI. After processing by EMD, the signal consists of a stationary response of a single mode. Thus, this approach can take a full advantage of the SSI. There are some obviously stable axes in the stability diagram from this approach and modal parameters can be identified more precisely.

4.4 Case study based on the shaking table test data of a reinforced concrete frame model

In order to validate the applicability of the proposed approaches in restraining the end-effect in the EMD and to identify the modal parameters, recorded acceleration data from shaking table tests of a 12-story reinforced concrete frame model at 1/10 scale (Lu *et al*., 2004) are taken as the case study. The model beam is 30 mm×60 mm and column is 50 mm×60 mm; the thickness of floor slab is 12 mm. As shown in Fig. 1, accelerometers were positioned along the *X*, *Y* and *Z* directions. The El Centro record during the 1940 Imperial Valley earthquake, the Kobe record during 1995 Kobe earthquake and the Shanghai artificial ground motion record with different peak accelerations are selected as shaking table inputs.

The *X*-direction acceleration data at gauge point A7 from the case under El Centro record excitation with peak acceleration 0.09g is used as an example. The acceleration signal from the gauge point A7 at the top floor is shown in Fig. 2. Fourier spectrum of the original signal is shown in Fig. 3.

The original signal is preprocessed through a band-pass filter and predicted via RBF neural network and mirror extension. Then, EMD is performed on each preprocessed signal. The EMD results of the filtered acceleration signal at gauge point A7 that deal with and without end-effect are shown in Fig. 4, respectively. After preprocessing, 7 IMFs are obtained and distortion at the ends of all IMFs is obviously decreased.

After decomposing by EMD, modal responses $x_j'(t)$ (j=1,2...) can be obtained. The 1st modal response $x_1'(t)$ is processed through RDT and the free-decay response $x_1''(t)$ is obtained, as shown in Fig. 5. The free-decay response $x_1''(t)$ of the 1st mode is also obtained through NExT, which is shown in Fig. 6.

Each free-decay response is performed by Hilbert transform. The frequency and damping ratio of each mode can be identified by the approaches above. The phase of the free-decay response of the 1st mode obtained through EMD and RDT is shown in Fig. 7. The instantaneous frequency ω_1 of the 1st mode is shown in Fig. 8. Figures 9 and 10 show the $\ln A_1(t)$–t curves and their linear least-squares fitting from HHT and RDT, and HHT and NExT, respectively. Using the same methods, modal parameters of the other modes can be identified.

A stability diagram through SSI with EMD is shown in Fig. 11. It seems that the method using SSI and EMD is reliable because the real model is the one whose frequency does not change when system orders are selected differently.

The identified modal frequencies of the first three modes and a comparison with the results from eigensystem realization algorithm (ERA), rational fraction polynomial (RFP) and finite element analysis are shown in Table 1. The identified modal damping ratios of the first three modes and a comparison with the results from the other identification approaches are shown in Table 2 (Han *et al*., 2009). It is obvious that the identified frequencies from ERA and FRP are less

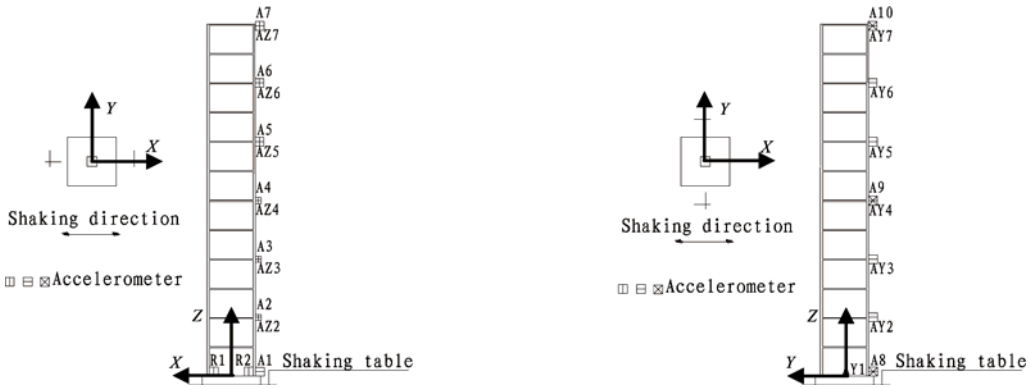

(a) Parallel to the shaking direction (b) Perpendicular to the shaking direction

Fig. 1 Position of accelerometers in the shaking table model

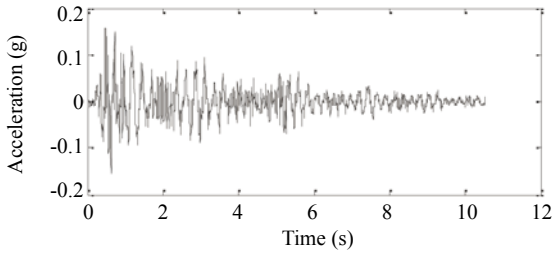

Fig. 2 Original *x*-direction acceleration signal at gauge Point A7

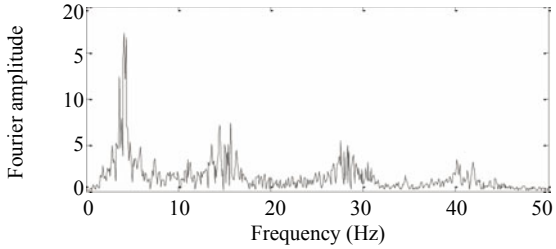

Fig. 3 Fourier spectrum of the original signal at gauge Point A7

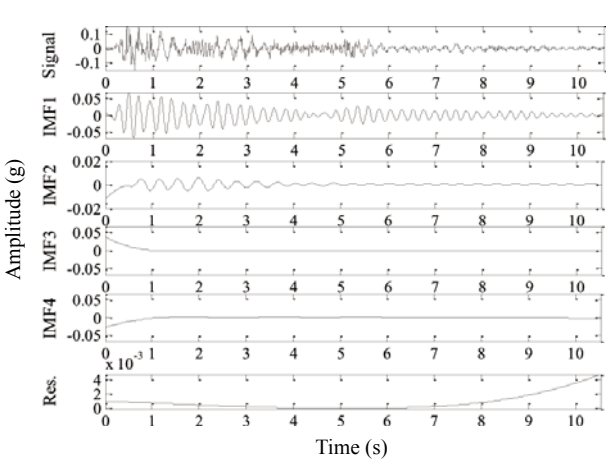

(a) Without preprocessing

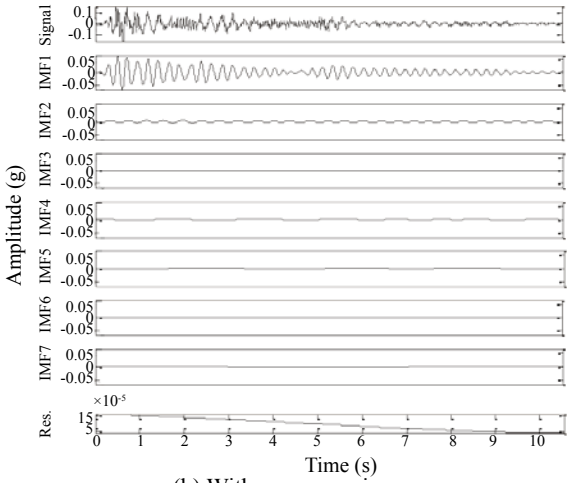

(b) With preprocessing

Fig. 4 EMD results of the filtered acceleration signal without and with preprocessing combining RBF neural network prediction with mirror extension

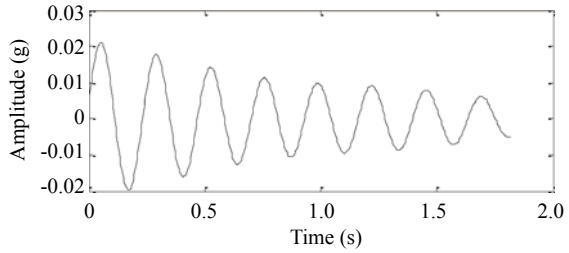

Fig. 5 Free-decay vibration response $x''_1(t)$ of 1st mode from EMD and RDT

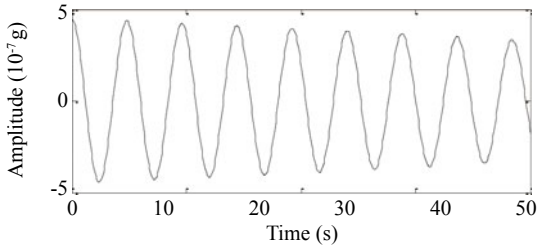

Fig. 6 Free-decay response $x''_1(t)$ of the 1st mode from EMD and NExT

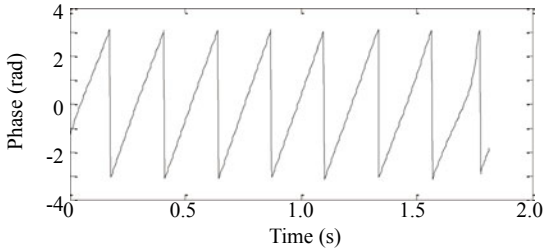

Fig. 7 Phase of the free-decay response of the 1st mode from RDT and HHT

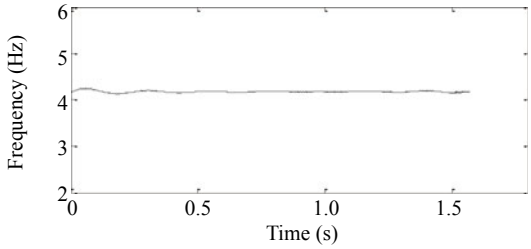

Fig. 8 Instantaneous frequency ω_1 of the 1st mode

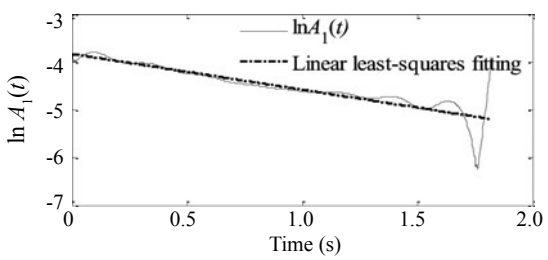

Fig. 9 $\ln A_1(t)$–t curve of $x''_1(t)$ from HHT and RDT and its linear least-squares fitting

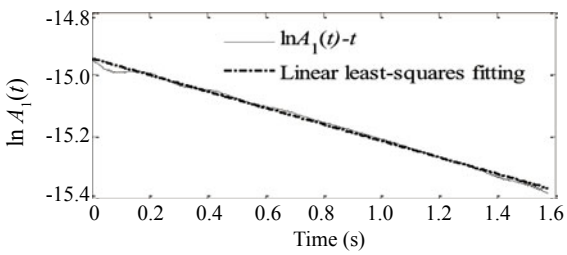

Fig. 10 $\ln A_1(t)$–t curve of $x''_1(t)$ from HHT and NExT and its linear least-squares fitting

Table 1 Identified modal frequencies and comparison with the results from the other identification approaches and finite element analysis

Mode No.	Modal frequency (Hz)						
	HHT+RDT	HHT+NExT	EMD+SSI	ERA	RFP	FFT	FEM
1	3.76	4.17	4.32	3.56	3.55	4.18	3.80
2	14.33	14.56	14.79	14.08	13.96	14.52	14.43
3	27.48	27.99	27.82	27.18	27.17	27.61	27.82

Table 2 Identified modal damping ratios and comparison with the results from the other identification approaches

Mode No.	Modal damping ratio (%)					
	HHT+RDT	HHT+NExT	EMD+SSI	ERA	RFP	FFT
1	3.87	6.80	1.66	5.93	5.46	11.91
2	2.51	6.37	1.81	4.14	4.80	5.81
3	1.93	4.89	1.69	3.69	3.81	4.68

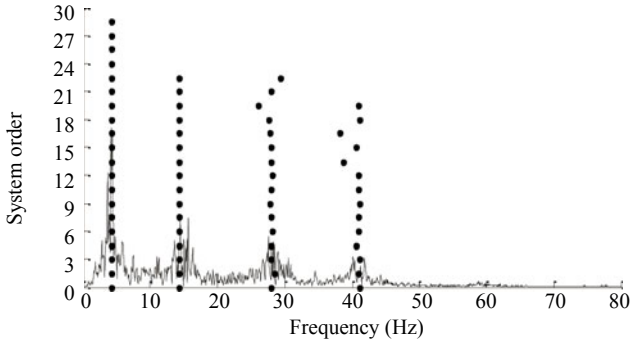

Fig. 11 Stability diagram using SSI and EMD

than the results from a simple FFT. It also indicates that stiffness of the structure is underestimated using ERA and RFP. Inversely, comparison between the identified frequencies from the proposed methods and those from simple FFT indicates that the proposed approaches are more reliable in identifying modal frequencies. For the modal damping ratios, although the identified results are improved by comparison with the half-power bandwidth method, there is an obvious difference in the results of the different identification approaches.

5 Structural damage diagnosis methods based on the HHT

5.1 Damage evolution identification via instantaneous frequency and instantaneous energy

When structural damage occurs, stiffness degradation inevitably leads to a change of vibration frequency. Damage evolution can be identified by investigating frequency changes of the structure. In addition, energy transformation characteristics during the structural damage process can be reflected by analyzing Hilbert instantaneous energy of input and output of the structure.

5.2 Damage location identification via the relative amplitude of Hilbert marginal spectrum

The Hilbert-Huang spectrum describes the signal amplitude and reflects the energy distribution of vibration signals in the time-frequency domain. And, the Hilbert marginal spectrum $h(\omega,x)$ reflects signal amplitude changes in the frequency domain. It also can show the energy contribution of different frequency components in the whole time domain. Consequently, damage locations can be identified by comparing the relative amplitudes of Hilbert marginal spectra at all gauge points before and after damage.

5.3 Case study based on shaking table model test data

5.3.1 Damage evolution identification of the model structure

The acceleration signals of the 12-story reinforced concrete frame model at gauge Point A7 under the excitation cases of No. 2, 8, 17, 26, 35, 44 and 53, in which peak acceleration of the NS component at El Centro station (1940) were scaled to the corresponding values shown in Table 2, is used as an example. The signals under these cases are supposed to be sampled continuously. The filtered acceleration signal is shown in Fig. 12 with appropriate cut-off frequencies. The first four IMFs by processing the filtered acceleration signal with EMD are shown in Fig. 13.

The Hilbert-Huang spectrum obtained by

Table 3 Peak table acceleration under Case No. 2, 8, 17, 26, 35, 44 and 53

Case No.	2	8	17	26	35	44	53
Peak table acceleration (g)	0.090	0.258	0.388	0.517	0.646	0.775	0.904

transforming IMF1 is shown in Fig. 14. It shows the 1st modal frequency has an obvious drop at 21s and 32s. This indicates that structural damage occurred during the 17th excitation and continued as the excitation increased. This shows good agreement with the experimental observation (Lu *et al*., 2004).

The Hilbert instantaneous energy of input and output are shown in Fig. 15. From Fig. 15, it is seen that input with relatively lower energy caused a larger energy response of the structure before 42s. But after 42s, the Hilbert instantaneous energy of output is significantly reduced under the higher excitation. At 53s, the Hilbert instantaneous energy amplitude of output is 1.184×10^5 while its input is 3.705×10^5. This result shows that the developing structural damage converts the stiff model structure to be soft. This softening increases deformation and dissipates a large amount of input energy. This also shows good agreement with the experimental observation. During the shaking table test, vertical cracks propagated at the beam end after the 17th excitation. The cracks continued growing and the number of cracked beams also increased as the input excitation increased (Lu *et al*., 2004).

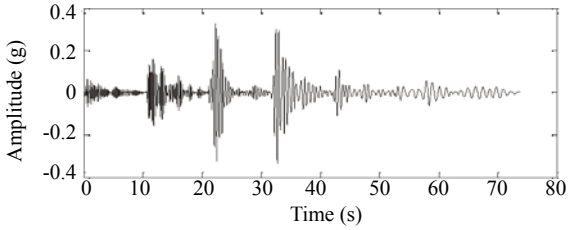

Fig. 12 Filtered acceleration response with supposed continuous sampling at gauge Point A7

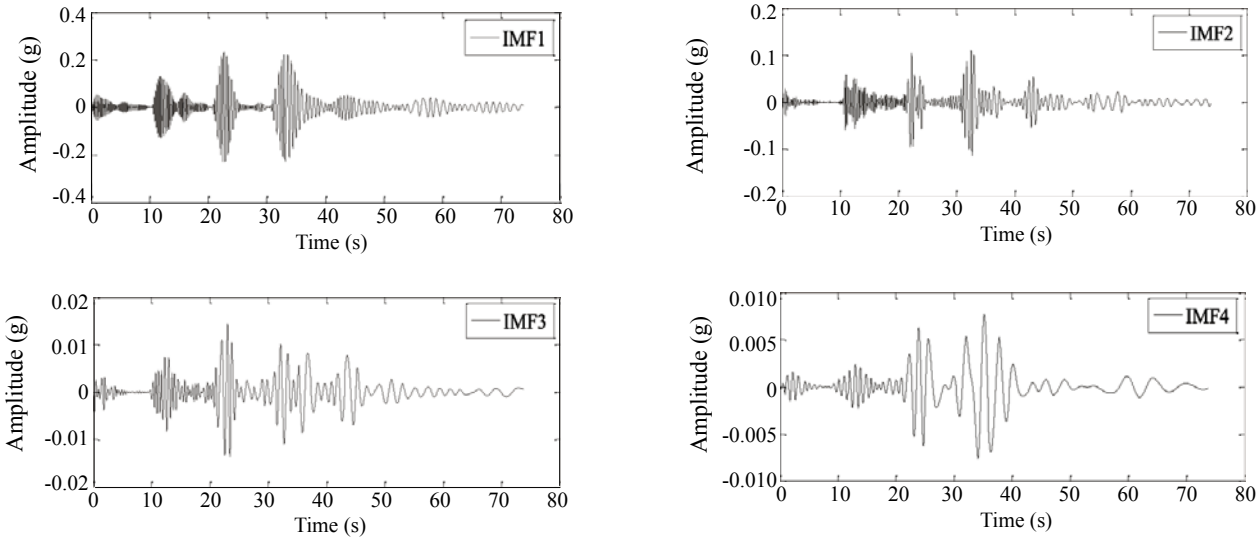

Fig. 13 EMD results of filtered acceleration response at gauge Point A7

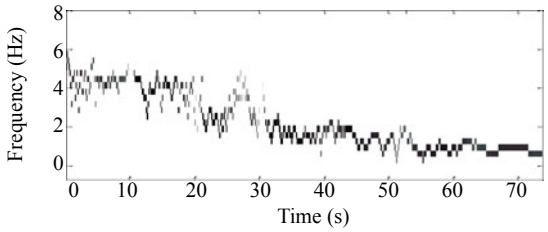

Fig. 14 Hilbert-Huang spectrum of filtered acceleration response at A7

5.3.2 Damage location identification of the model structure

Experimental results show that no cracks were found on the model structure under the first seven excitation

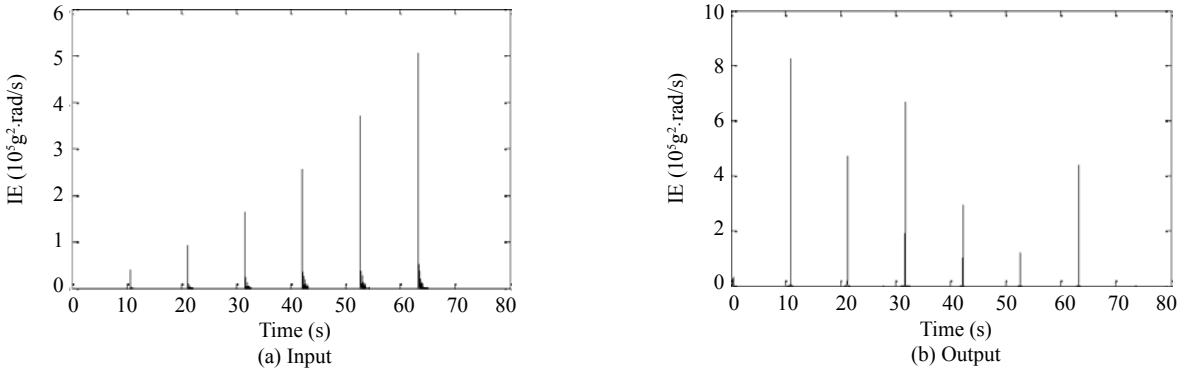

Fig. 15 Hilbert instantaneous energy of input and output

Table 4 Peak table acceleration under Case No. 7, 8, 9 and 10

Case No.	7	8	9	10
Original ground motion record	White noise	El Centro, 1940	Kobe, 1995	Shanghai artificial ground motion
Peak table acceleration (g)	0.090		0.258	

Table 5 Absolute and relative amplitudes of Hilbert marginal spectra at A3, A4, A5 and A6 gauge points under 4 excitation cases

Gauge point/Floor		A3 / 5	A4 / 7	A5 / 9	A6 / 11
Under the 7th excitation	Absolute	8.9420	14.6300	19.4300	22.23
	Relative	0.4022	0.6581	0.8740	1.00
Under the 8th excitation	Absolute	15.1800	25.3700	33.3100	37.97
	Relative	0.3998	0.6681	0.8773	1.00
Under the 9th excitation	Absolute	47.7700	80.8000	107.1000	119.20
	Relative	0.4008	0.6778	0.8985	1.00
Under the 10th excitation	Absolute	5.4870	13.5000	18.8800	21.00
	Relative	0.2602	0.6401	0.8952	1.00

cases and fine cracks occurred at the end of the 4th floor frame beam after the 9th excitation case. Thus, the acceleration response signals of the A3, A4, A5 and A6 gauge points under the 7th, 8th, 9th and 10th excitations as shown in Table 4 are selected to verify the capability to identify damage location by the relative amplitudes of the Hilbert marginal spectra.

Relative amplitudes of the Hilbert marginal spectra at A3, A4, A5 and A6 gauge points under four excitation cases, respectively, are shown in Fig. 16. Absolute and relative amplitudes of the Hilbert marginal spectra at these four gauge points under different excitations are shown in Table 5. Figure 16 and Table 5 show that there is little change in the relative amplitudes of the Hilbert marginal spectrum at the A3, A4, A5 and A6 gauge points from the 7th excitation to the 9th excitation. But there is obvious change at the A3 gauge point between the 9th and 10th excitation. This agrees well

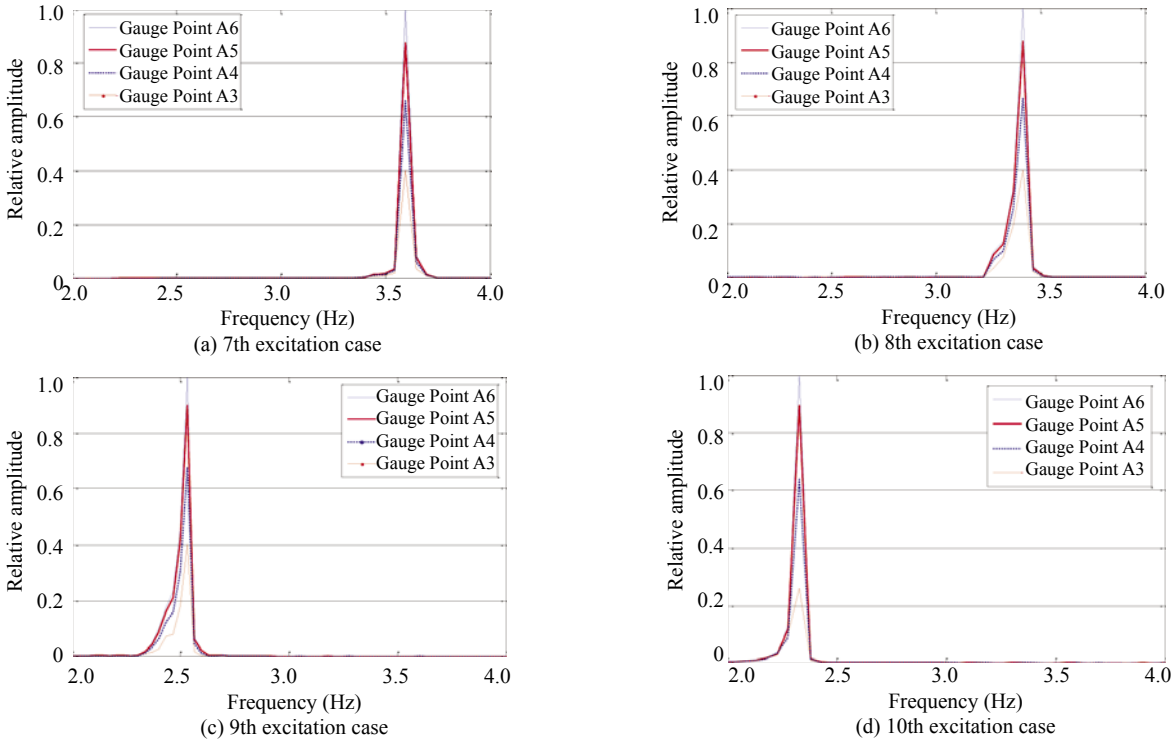

Fig. 16 Relative amplitudes of Hilbert marginal spectra at A3, A4, A5 and A6 gauge points under 4 excitation cases

with the experimental observations (Lu *et al*., 2004). This indicates that relative amplitudes of the Hilbert marginal spectra can reflect the energy distribution of the vibrating structure. Thus, damage locations in the structure can be identified by comparing relative amplitudes of the Hilbert marginal spectra before and after structural damage.

6 Conclusions

In this study, modal parameter identification approaches and damage diagnosis methods, which are all based on HHT, are proposed. Acceleration records at gauge points from shaking table tests of a 12-story reinforced concrete frame model are processed, and modal parameter identification and damage diagnosis of the model structure are conducted. The proposed approaches based on HHT have their own obvious advantages in identifying modal parameters because the stationary data which contained the modal response signal of the single mode are obtained through EMD. In addition, in this study, mirror extension and prediction via a radial basis function (RBF) neural network are used to restrain the troublesome end-effect issue in EMD. Modal parameters from the proposed approaches are more reliable. A comparison of the identification results with the results from the other identification algorithms, such as ERA and RFP, and finite element analysis indicates that the proposed approaches are reliable to identify modal frequencies. Although identification of modal damping ratios is improved by comparison with the half-power bandwidth method, it is still difficult to confirm the precision of the results.

Damage evolution of the structure is identified by investigating the time-varying characteristics of instantaneous frequency and comparing Hilbert instantaneous energy of input and output. The damage location of the structure is identified directly by comparing relative amplitudes of the Hilbert marginal spectra before and after the damage. Damage evolution and damage location are very easy and simple to identify with the proposed methods and they show good agreement with the experimental observations.

In conclusion, HHT and the approaches based on HHT are promising in modal parameter identification and damage diagnosis, and can be applied in the field of structural health monitoring. However, further studies are needed in order to precisely identify the damping ratios.

References

Caicedo JM, Dyke SJ and Johnson EA (2004), "Natural Excitation Technique and Eigensystem Realization Algorithm for Phase I of the IASC-ASCE Benchmark Problem: Simulated Data," *Journal of Engineering Mechanics*, **130**: 49–60.

Chen B, Xu YL and Qu WL (2005), "Evaluation of Atmospheric Corrosion Damage to Steel Space Structures in Coastal Areas," *International Journal of Solids and Structures*, **42**(16): 4673–4694.

Curadelli RO, Riera JD, Ambrosini D and Amani MG (2008), "Damage Detection by Means of Structural Damping Identification," *Engineering Structures*, **30**: 3497–3504.

Doebling SW, Farrar CR, Prime MB and Shevitz DW (1996), "Damage Identification and Health Monitoring of Structural and Mechanical Systems from Changes in Their Vibration Characteristics: A Literature Review," Los Alamos National Laboratory, Los Alamos, New Mexico.

Farrar CR and Jauregui DA (1998), "Comparative Study of Damage Identification Algorithms Applied to a Bridge: I Experiment," *Smart Materials and Structures*, **7**: 704–719.

Han JP, Lu XL and Wang FX (2009), "Comparison of Modal Parameter Identification Algorithms Based on Shaking Table Model Test Data," *Proc. of SPIE*, **7375**: 73750K-1–7.

Han JP, Qian J and Dong XJ (2010), "Suppression of end-Effect in Empirical Mode Decomposition by Mirror Extension and Radial Basis Function Neural Network Prediction," *Journal of Vibration, Measurement & Diagnosis*, **30**(4): 414–417, 474.

Hsu WK, Chiou DJ, Chen CW, Liu MY, Chiang WL and Huang PC (2013), "Sensitivity of Initial Damage Detection for Steel Structures Using the Hilbert-Huang Transform Method," *Journal of Vibration and Control*, **19**: 857–878.

Huang NE, Shen Z, Long SR, Wu MC, Shih HH, Zheng Q, Yen NC, Tung CC and Liu HH (1998), "The Empirical Mode Decomposition and the Hilbert Spectrum for Nonlinear and Non-stationary Time Series Analysis," *Proceedings of the Royal Society A: Mathematical, Physical and Engineering Sciences*, **454**: 903–995.

Ibrahim SR (1977), "Random Decrement Technique for Modal Identification of Structures," *Journal of Spacecraft and Rockets*, **14**: 696–700.

Liu TY, Chiang WL Chen CW, Hsu WK, Lin CW, Chiou DJ and Huang PC (2012), "Structural System Identification for Vibration Bridges Using the Hilbert-Huang Transform," *Journal of Vibration and Control*, **18**: 1939–1956.

Lu XL, Li PZ and Chen YQ (2004), *Complete Data of Shaking Table Test on a 12-story Reinforced Concrete frame Model*, State Key Laboratory of Disaster Reduction in Civil Engineering, Tongji University, Shanghai. (in Chinese)

Rilling G, Flandrin P and Goncalves P (2003), "On Empirical Mode Decomposition and Its Algorithms," *IEEE-EURASIP Workshop on Nonlinear Signal and*

Image Processing, *NSIP-03*, 1–5.

Van Overschee P and De Moor B (1996), *Subspace Identification for Linear Systems: Theory-implementation-applications*, Kluwer Academic Publishers, Boston.

Yang JN and Lei Y (2000), "Identification of Tall Building Using Noisy Wind Vibration Data," *Proc. of the International Conference on Advances in Structural Dynamics*, Hongkong, China.

Yu D and Ren W (2005), "EMD-based Stochastic Subspace Identification of Structures from Operational Vibration Measurements," *Engineering Structures*, **27**: 1741–1751.